J Appl Electrochem (2013) 43:541–551
DOI 10.1007/s10800-013-0538-1

ORIGINAL PAPER

Zinc deposition and dissolution in sulfuric acid onto a graphite–resin composite electrode as the negative electrode reactions in acidic zinc-based redox flow batteries

Junli Pan · Yuehua Wen · Jie Cheng · Junqing Pan · Zhangli Bai · Yusheng Yang

Received: 9 January 2013 / Accepted: 25 February 2013 / Published online: 8 March 2013

Abstract Electrodeposition and dissolution of zinc in sulfuric acid were studied as the negative electrode reactions in acidic zinc-based redox flow batteries. The zinc deposition and dissolution is a quasi-reversible reaction with a zinc ion diffusion coefficient of 4.6×10^{-6} cm^2 s^{-1} obtained. The increase of acid concentration facilitates an improvement in the kinetics of zinc electrodeposition–dissolution process. But too high acid concentration would result in a significant decrease in charge efficiency. The performance of the zinc electrode in a three-electrode system with magnetic stirring was also studied as a function of Zn(II) ion concentration, sulfuric acid concentration, current density, and the addition of additives in 1 M H_2SO_4 medium. The optimum electrolyte composition is suggested at high zinc(II) concentration (1.25 M) and moderate sulfuric acid concentration (1.0–1.5 M) at a current density range of 20–30 mA cm^{-2}. Whether in acid-free solution or in sulfuric acid solution with or without additives, no dendrite formation is observed after zinc electrodeposition for 1 h at 20 mA cm^{-2}. The energy efficiency is improved from 77 % in the absence of additives in 1 M H_2SO_4 medium to over 80 % upon the addition of indium oxide or SLS–Sb(III) combined additive as hydrogen suppressants.

Keywords Zinc electrodeposition and dissolution · Sulfuric acid · Additive · Zinc-based redox flow battery

J. Pan · J. Pan · Z. Bai · Y. Yang
College of Science, Beijing University of Chemical Technology, Beijing 100029, China

Y. Wen (✉) · J. Cheng · Y. Yang
Research Institute of Chemical Defence, Beijing 100191, China
e-mail: wen_yuehua@126.com

1 Introduction

Due to the rapid growth of wind, solar, and other renewable energy sources, increasing attention has been given to the development of more advanced, reliable, and safer redox flow batteries (RFB) [1]. Since 1970, a number of systems have been investigated for use in RFB technology. Great attention has been paid to the following main systems such as Fe–Cr battery, all-vanadium battery, Zn–Br_2 battery, and Zn–Ni single flow battery. Due to its low equilibrium potential, good reversibility, low cost, high energy density, and environmental friendliness, the zinc electrode has been used for a wide variety of applications as a negative electrode in secondary batteries [2]. The large negative potential of the zinc electrodes allows a high voltage and high energy density when coupled with other electropositive redox couples. Meantime, the battery performance also depends on the type of electrolyte used.

In the mid-1970s to early 1980s, Exxon and Gould corporations designed Zn–Br_2 flow batteries in weakly acidic medium [3], which allowed the development of the zinc-based batteries to be commercialization. Since 2007, two types of zinc-based redox flow battery systems in alkaline medium were proposed by us, namely, single flow zinc–nickel battery [4] and zinc–air battery using zinc regeneration electrolysis with propanol oxidation as a counter electrode reaction [5]. Unlike the solid zinc electrodes in conventional Zn–Ni secondary batteries, the reaction of zinc electrodes in RFBs is turned into the zinc deposition and dissolution. Further, the use of flowing electrolytes provides an effective approach to suppress dendritic growth, shape change, and passivation of zinc electrodes [3, 6]. However, spongy zinc deposition is still easy to be formed from flowing solutions. This maybe attributed to the high activity of zinc in alkaline medium

and the change of the acidity in weakly acidic medium. Thus, the performance of batteries is influenced to a significant degree. Recently, a zinc–cerium flow battery was proposed by Leung et.al. The design of this battery is similar to that of Zn–Br_2 flow batteries [7–9]. However, to prevent self-discharge of the cell, an ion exchange membrane must be used to separate the positive and negative electrodes. Moreover, effect of the support electrolyte, methanesulfonic acid, on the solubility of Ce(III) ions is contrary to that on the solubility of Ce(IV) ions. The acidity of the electrolyte often changes during charge–discharge cycles, which leads to poor stability of the zinc electrodes in acidic medium.

Zinc electrodeposition has been practiced for a long time using acidic chloride [10, 11] and sulfate [12–16] baths in the electroplating industry. The electrocrystallization of zinc is sensitive to the zinc concentration [11] as well as the identity of additives [12–16]. Organic additives such as surfactants, are commonly used in zinc electrodeposition to control the metallic crystal shape and size, in order to produce smooth and bright deposits [14–16]. Common effects of the organic additives are changes in the preferred deposit orientation, morphology, and an increase in the deposition overpotential due to the adsorption of additives at the electrode surface. Further, the surface morphology of deposits is also strongly correlated to deposit texture. A glassy carbon, carbon steel, or platinum can be employed as substrates for the zinc electrodeposition from an acidic chloride solution. For the zinc electrodeposition from an acidic sulfate solution, stainless steel, and aluminum are usually used as substrates. On the other hand, pulse plating was used to improve the morphology and properties of the deposits for zinc deposition from chloride or sulfate electrolytes in the presence of additives [17, 18]. Up to now, there have been few studies of zinc electrodeposition and dissolution from sulfuric acid electrolytes in the application of batteries. Fang has discussed the electrochemical behavior of the Ce(III)/Ce(IV) redox couple in sulfuric acid medium [19]. Relatively low H_2SO_4 concentration is favorable electrochemically for the Ce(III)/Ce(IV) redox couple, which is also beneficial for the zinc deposition and dissolution process. Also, the electrode potential of Ce(III)/Ce(IV) redox couple is slightly shifted to a negative value as Ce^{3+} and Ce^{4+} are easy to complex with SO_4^{2-}, attenuating greatly the effect of oxygen evolution. And then, the combination of the zinc redox couple with Ce(III)/Ce(IV) couple in sulfuric acid medium can be expected to obtain higher energy efficiency and better charge–discharge cycling stability, being an attractive system. In addition, when the Zn/Zn^{2+} redox couple is coupled with the $PbO_2/PbSO_4$ electrode, no membrane is needed and the cell potential is also higher.

In this work, the electrochemistry of zinc in sulfuric acid was studied via cyclic voltammetry at a graphite–resin composite electrode. The kinetic characterization of the Zn^{2+}/Zn redox couple in sulfuric acid medium was determined by cathodic potentiodynamic polarization measurements (log *i*–*E*). In order to optimize the conditions for zinc-based redox flow batteries, a range of zinc electrodeposition and dissolution experiments have been carried out in a three-electrode flow-cell with magnetic stirring using different electrolyte compositions and current densities. A detailed discussion of zinc morphology and charge–discharge efficiency in the presence and absence of additives is included.

2 Experiments

Cyclic voltammetry was carried out in a three-electrode cell. The working electrode was a graphite–resin composite electrode (area: 0.14 cm^2, Heixia Carbon Products Limited Company, Shanghai, China), while the counter electrode was a large area lead sheet (projected area: 10 cm^2). For the cyclic voltammetry, the potential was linearly swept from −1.0 to −1.9 V versus $Hg|Hg_2SO_4$ at a potential sweep rate in the range from 5 to 100 mV s^{-1}. Cyclic voltammograms were recorded over a wide range of electrolyte composition including 0.01–0.4 M zinc sulfate in 0.5 M sodium sulfate solution adjusted to pH 4.

Charge–discharge of zinc electrodes in sulfuric acid was carried out in a three-electrode cell with magnetic stirring. A graphite–resin composite (area: 2 × 2 cm^2) was used as the working electrode. Two sheets of $PbO_2/PbSO_4$ solid electrode with an area of 4.5 × 5 cm^2 were used as counter electrodes. Zinc was electrodeposited at current densities in the range of 10–50 mA cm^{-2} for 1 h, followed by zinc dissolution using the same current density. The zinc dissolution stopped when the zinc half-cell voltage shifted toward a more positive value than −1.2 V versus $Hg|Hg_2SO_4$. The pH of 1.25 M $ZnSO_4$ solution is about 4. The pH of the other solutions with various concentrations of H_2SO_4 is closed to 0 or below 0. Log *i* versus *E* curves of 1.25 M Zn(II) were obtained in a positive going direction over the range from −1.6 to −1.3 V versus Hg/Hg_2SO_4 in sulfuric acid solution with various concentrations at a scan rate of 1 mV s^{-1}. The cell assembly was the same as that in the cyclic voltammetry experiment. The anodic and cathodic linear segments of Log *i*–*E* curves gave the respective Tafel slopes. The electrode potential was measured against a Hg/Hg_2SO_4 electrode. All electrochemical measurements were made with an electrochemical working station (Solartron 1280z).

Zinc electrodeposition in the presence and absence of additives and acid was carried out in an electrolyte containing 1.25 M zinc sulfate. The applied current density was 20 mA cm^{-2} for 1 h. A graphite–resin composite

electrode of 2 cm × 2 cm dimension was used as the substrate for zinc electrodeposition. Before each experiment, the electrodes were polished using silicon carbide paper (grade P1000), and cleaned in de-ionized water. Throughout the experiment, the solution was stirred using a magnetic stirrer. After the electrodeposition, samples were rinsed with ultrapure water for 30 s, vacuum-dried and stored in a sample bag placed in a desiccator. The images of the zinc electrodeposits were obtained with a scanning electron microscope (model APollo300).

3 Results and discussion

3.1 Cyclic voltammetry

3.1.1 Effect of zinc concentration

Figure 1a shows a typical cyclic voltammogram obtained from a solution of 0.01 M $ZnSO_4$ + 0.5 M Na_2SO_4 on a graphite–resin composite electrode. The potential was firstly swept from −1.0 to −1.9 V versus Hg|Hg_2SO_4. The voltammogram main features are the sharp cathodic reduction peak and the corresponding anodic stripping peak, which is similar to those reported in methanesulfonic acid medium [7]. A voltammogram obtained in the absence of Zn^{2+} ions is also presented. The comparison of voltammograms obtained in the presence and absence of Zn^{2+} ions suggests that hydrogen evolution occurs at about −1.86 V versus Hg|Hg_2SO_4 which is negative than the electrode potential of zinc deposition. It indicates that the H_2 overpotential is large on the graphite–resin composite electrode, which facilitates the deposition of zinc ions. While sweeping the potential toward the positive direction, a crossover characteristic of nucleation processes was observed. The forward and reverse scans form a relatively large nucleation loop between −1.59 and −1.54 V versus Hg|Hg_2SO_4, which is similar to those reported about zinc deposition on carbon electrodes [7, 11] and a platinum electrode [10]. The second potential is known as the crossover potential (E_{co}). In this loop, the Zn(II) reduction current density during the forward scan is lower than that during the reverse scan. It indicates that the

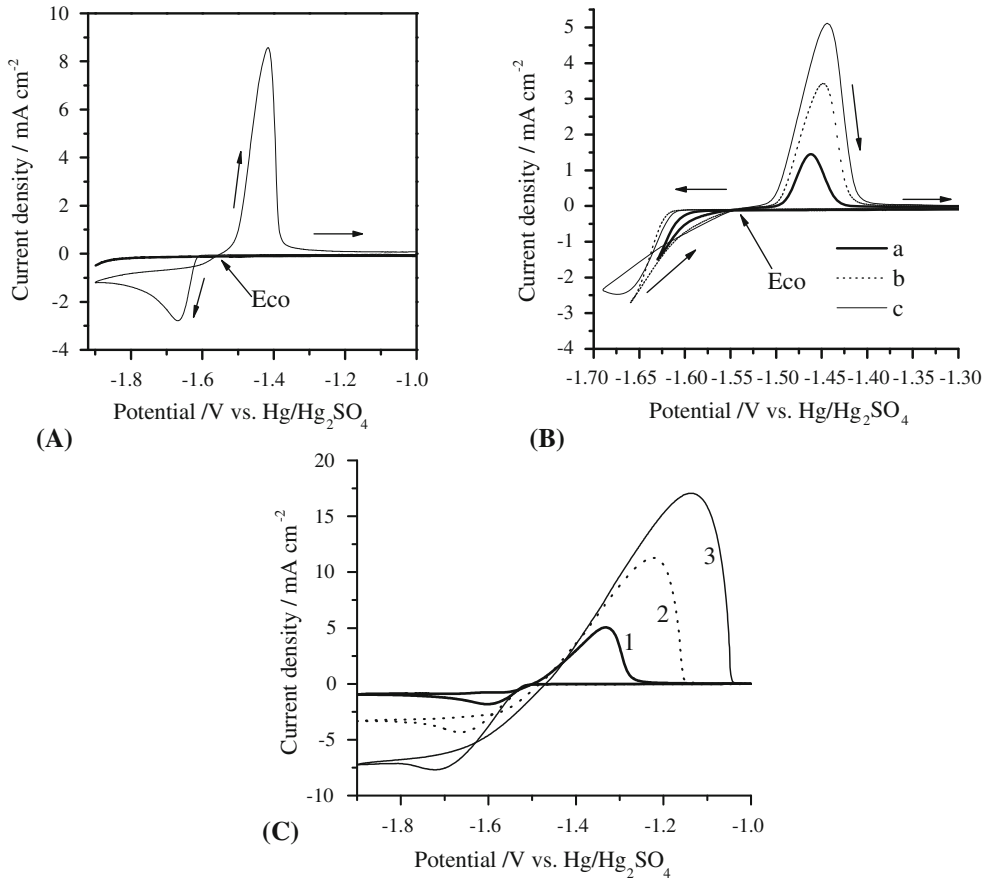

Fig. 1 **a** Cyclic voltammograms obtained for a graphite–resin composite electrode in 0.01 M $ZnSO_4$ + 0.5 M Na_2SO_4 (*full line*) and 0.5 M Na_2SO_4 (*heavy full line*). **b** Typical voltammograms for zinc nucleation in a solution of 0.01 M $ZnSO_4$ + 0.5 M Na_2SO_4 at different switching potentials (E_λ). E_λ : *a* −1.63 V; *b* −1.66 V; *c* −1.69 V vs. Hg/Hg_2SO_4. **c** Variation of the cyclic voltammogram of Zn(II) ions with the Zn(II) concentration in 0.5 M Na_2SO_4 solution. Concentration of Zn(II): *1* 0.1 M; *2* 0.2 M; *3* 0.4 M. Scan rate: 30 mV s − 1

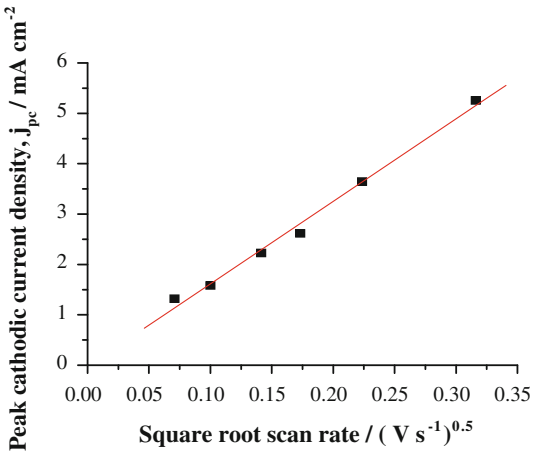

Fig. 2 Variation of the cathodic peak current density with the square root of the potential sweep rate for a graphite–resin composite electrode in the electrolyte of 0.01 M $ZnSO_4$ + 0.5 M Na_2SO_4, using potential sweep rates of 5, 10, 20, 30, 50, and 100 mV s^{-1}

deposition of zinc on the graphite–resin composite substrate required slightly more energy than that on the freshly deposited zinc surface.

The behavior of E_{co} was studied in order to establish the type of kinetic control during the growth of the nuclei. For this study, the switching potential (E_λ) is fixed at the foot of the reduction peak of Zn(II). Figure 1b shows the effect of varying the switching potential (E_λ) on cyclic voltammograms under these conditions. When E_λ is successively switched in the potential range −1.63 to −1.69 V versus Hg/Hg_2SO_4, the value of E_{co} remains constant. A similar result was obtained by Gomes et al. [14] for Zn electrodeposition on steel in sulfate medium. According to the Fletcher theory [11, 20], the growth rate of the nuclei is independent on the nucleation time. That means that the nuclei growth rate is under charge transfer control not diffusion control.

In terms of electron transfer, the zinc deposition reaction in a sulfate bath is considered to be a quasi-reversible reaction, as the separation of peak potentials was about 200 mV in an electrolyte containing 0.01 M Zn(II) ions. This value is larger than the separation of peak potentials for the Zn(II)/Zn(0) reaction reported in literatures maybe due to effect of different anions in electrolytes [21]. Increasing the Zn(II) concentration to 0.4 M, variation of the cyclic voltammograms on a graphite–resin composite electrode with the Zn(II) concentration is shown in Fig. 1c. It can be seen that with the concentration of Zn(II) increasing, the reduction peak becomes less sharp, tending to be a plateau of limiting diffusion current. It is possibly indicative of the relatively slow electrode kinetics or the fast diffusion rate of Zn(II) ions.

The influence of potential scan rate (v) on the Zn deposition in a solution of 0.01 M $ZnSO_4$ + 0.5 M Na_2SO_4 was measured. The relation between the cathodic peak current density and the square root of scan rate ($v^{1/2}$) is presented in Fig. 2. It can be seen that the peak current density increases linearly with the square root of the potential sweep rate, indicative of a mass transport controlled reaction. From the Randles–Sevcik equation, the diffusion coefficient for zinc ions was found to be 4.6 × 10^{-6} cm^2 s^{-1}, while Yu et al. [21] reported a value of 4.8 × 10^{-6} cm^2 s^{-1} in the same electrolyte.

3.1.2 *Effect of proton concentration*

As a supporting electrolyte, the concentration of sulfuric acid is of critical importance to the electrochemical behavior of zinc deposition and dissolution. Cyclic voltammograms for 1.25 M Zn(II) ions at a graphite–resin composite electrode as a function of sulfuric acid concentration are shown in Fig. 3, and is used to determine the nucleation overpotential (NOP, see Table 1). The NOP, which is the difference between the nucleation initial potential (E_{nu}, point 'B') and the crossover potential (E_{co}, point 'A') in Fig. 3, is defined in the previous literature [22]. NOP is regarded as an indicator of the extent of polarization of a cathode, and high NOP values indicate

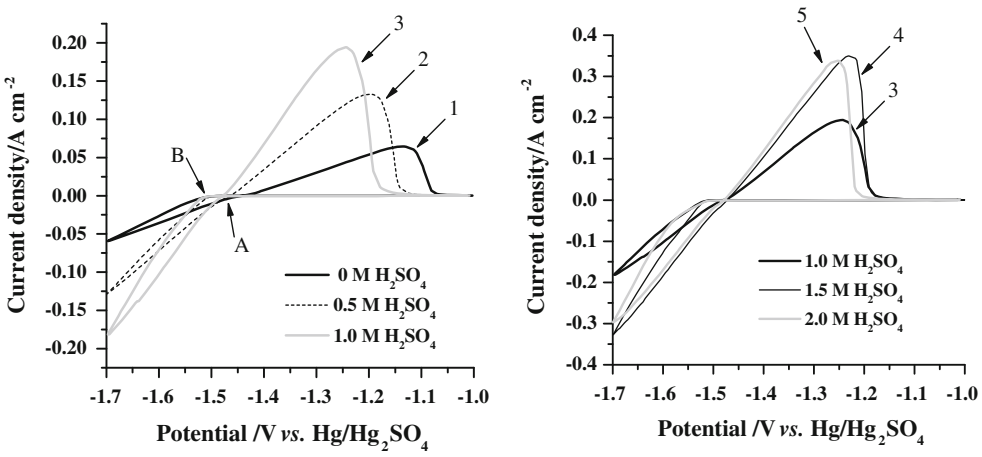

Fig. 3 Cyclic voltammograms for 1.25 M Zn(II) ions at a graphite–resin electrode as a function of sulfuric acid concentration at a scan rate of 30 mV s^{-1}. Concentration of H2SO4, (1) 0 M, (2) 0.5 M, (3) 1.0 M, (4) 1.5 M, and (5) 2.0 M

Table 1 Effects of the concentration of H_2SO_4 on nucleation potential (E_{nu}), nucleation overpotential (NOP), and dissolution peak potential (E_{dis}), anodic peak current density (I_{ac}) during zinc electrodeposition/dissolution from acidic sulfate solution

$C_{H_2SO_4}$ (M)	Cathodic deposition		Anodic dissolution	
	E_{nu} (V)	−NOP (mV)	E_{dis} (V)	I_{ac} (A cm^{-2})
0	−1.49	57	−1.14	0.064
0.5	−1.50	36	−1.20	0.132
1.0	−1.51	32	−1.24	0.195
1.5	−1.51	38	−1.23	0.350
2.0	−1.51	29	−1.25	0.338

All potential is referred to Hg/Hg_2SO_4

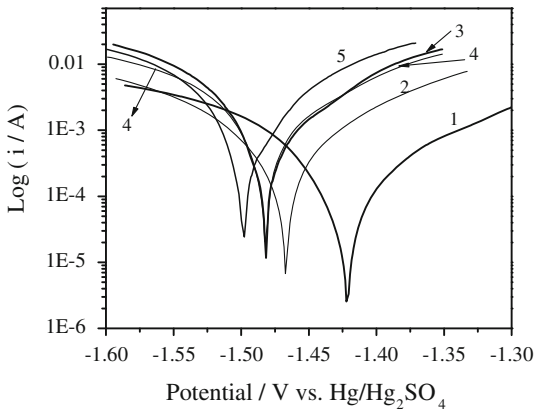

Fig. 4 Log *i–E* curves for 1.25 M Zn(II) ions in H_2SO_4 solution with various concentrations at a graphite–resin composite electrode (area: 0.14 cm^2). Concentration of H_2SO_4, *1* 0 M, *2* 0.5 M, *3* 1.0 M, *4* 1.5 M, *5* 2.0 M

strong polarization of the cathode. Compared with the acid-free solution, a slightly negative shift in the nucleation initial potential and a decrease in the NOP are observed with an increase in the H_2SO_4 concentration. Moreover, a significant negative shift in anodic dissolution potential along with an increase in the anodic peak current is found with increasing the sulfuric acid concentration to 1.5 M. Log *i–E* curves for 1.25 M Zn(II) ions with various concentration of H_2SO_4 at a graphite–resin composite electrode are presented in Fig. 4. The anodic and cathodic Tafel slopes, b_a and b_c, and I_0 (exchange current density), the equilibrium potential, E_0, were calculated from the Log *i* versus *E* curves as shown in Table 2. With the addition of 0.5 M H_2SO_4 in an aqueous solution of 1.25 M $ZnSO_4$, the exchange current density of zinc deposition and dissolution is enhanced one order of magnitude. And then, when the H_2SO_4 concentration is increased to above 1 M, almost no improvement in the exchange current density can be observed. It indicates the effect of proton, H^+, on the kinetics of zinc deposition and dissolution is limited when the H_2SO_4 concentration is beyond 1 M. At the same time, with increasing the H_2SO_4 concentration, a slight negative shift in the equilibrium potential is observed. Overall, there is no significant difference between anodic and cathodic Tafel slopes. The increase of proton concentration facilitates an improvement in the kinetics of zinc deposition–dissolution process, which may be attributed to higher conductivity of the electrolyte and an increase in the activity of zinc ions. However, hydrogen evolution and zinc corrosion become more serious due to increase in proton concentration. Therefore for the zinc deposition–dissolution in sulfuric acid medium, the H_2SO_4 concentration should not be too high. Therefore, the preferable H_2SO_4 concentration range should be 1–1.5 M.

3.1.3 *Effect of electrolytical additives*

Three kinds of electrolytical additives are selected from reports on the zinc electrowinning from sulfate electrolyte. Glutin [23] is a traditional organic additive used in the plating industry. Indium oxide [7] is an inorganic additive, while sodium lauryl sulfate (SLS) and Sb(III) [24] are organic and inorganic combined additive. Figure 5 shows the cyclic voltammograms for zinc electrodeposition and dissolution with the addition of selected additives in an electrolyte of 0.01 M $ZnSO_4$ + 0.5 M Na_2SO_4 at a graphite–resin composite electrode. The concentration of the additives was optimized values in literatures. The potential was firstly swept from −0.8 to −1.9 V versus $Hg|Hg_2SO_4$ and then reversed. It can be seen that in the presence of additives, the nucleation loop can still be observed except with indium oxide. But when indium oxide is used, the cathodic peak potential shifts to a more positive value, resulting in a significant decrease in the peak potentials

Table 2 Kinetics data of zinc deposition–dissolution at a graphite–resin composite electrode in sulfuric acid with different concentrations

Parameters	Without H_2SO_4	H_2SO_4			
		0.5 M	1 M	1.5 M	2 M
b_a (mV dec^{-1})	41.8	43.6	54.4	58.9	44.0
b_c (mV dec^{-1})	39.8	51.1	44.6	44.2	33.9
I_o (A cm^{-2})	3.0×10^{-4}	1.0×10^{-3}	2.7×10^{-3}	3.5×10^{-3}	2.3×10^{-3}
E_o (V)	−1.42	−1.47	−1.48	−1.48	−1.50

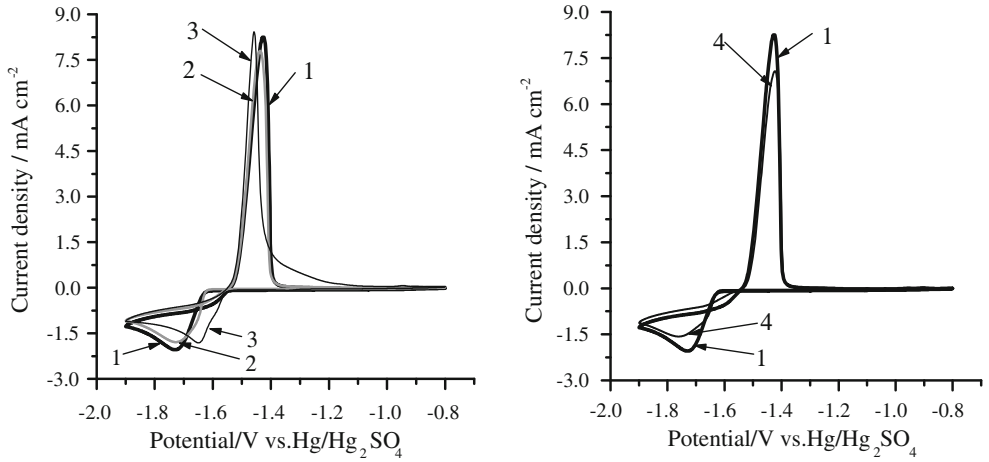

Fig. 5 Effect of additives on cyclic voltammograms of zinc electrodeposition and dissolution in acidic sulfate solution; electrolyte as in Fig. 1a : *1* no additive, *2* 1 mg L^{-1} SLS + 0.02 mg L^{-1}Sb (III), *3* 555 mg L^{-1} In_2O_3, *4* 50 mg L^{-1} glutin. Scan rate: 30 mV s^{-1}

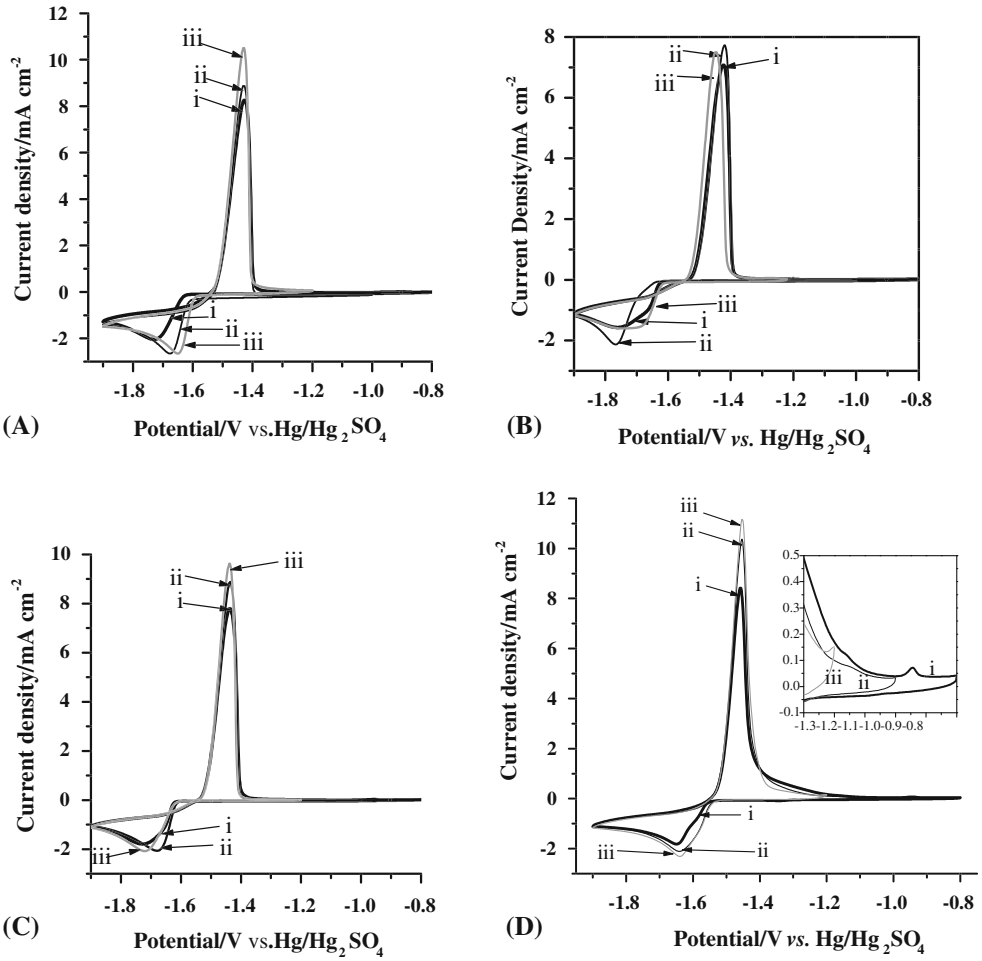

Fig. 6 The effect of initial scan potentials on cyclic voltammograms of zinc electrodeposition and dissolution in acidic sulfate solution; electrolyte as in Fig. 1a : **a** no additive, **b** 50 mg L^{-1} glutin, **c** 1 mg L^{-1} SLS + 0.02 mg L^{-1}Sb (III), **d** 555 mg L^{-1} In_2O_3. *inset* in **d**: the voltammograms with indium oxide in the potential range of −0.8 and −1.3 V vs. Hg/Hg_2SO_4. Initial potential: *i* −0.8 V, *ii* −1.0 V, *iii* −1.2 V vs. Hg/Hg_2SO_4. Scan rate: 30 mV s^{-1}

separation. The zinc cathodic and anodic peak currents also increase to a certain degree. This can be beneficial for the battery performance, as lower charge–discharge voltage difference can be expected due to the reduced overpotential. As a result, an improvement in the electrochemical behavior of zinc deposition and dissolution is the most remarkable

Table 3 Half-cell efficiencies of electrodeposition and stripping of Zn on a graphite–resin composite substrate from a sulfuric acid bath in a three-electrode cell with magnetic stirring

Operating parameter		Zinc overpotential, η (mV)	Zinc half-cell efficiency (%)		
			Charge	Voltage	Energy
Current density (mA cm^{-2})	10	111	51.79	92.70	48
	20	172	85.86	88.96	76
	30	198	88.8	87.42	78
	40	230	86.79	85.58	74
	50	307	90.77	81.18	74
H_2SO_4 concentration (M)	0	304	90.25	80.84	73
	0.5	199	86.05	87.29	75
	1	163	85.73	89.46	77
	1.5	135	84.82	91.28	77
	2	126	73.77	91.82	68
Zn^{2+} concentration (M)	0.8	187	81.72	88.08	72
	1.25	163	85.73	89.46	77
	1.5	218	87.28	86.07	75
	2	217	87.47	86.17	75
No additive		163	85.73	89.46	77
In_2O_3/555 mg L^{-1}		214	94.91	86.29	82
Glutin/50 mg L^{-1}		284	90.45	82.27	74
1 mg L^{-1} SLS + 0.02 mg L^{-1} Sb_2O_3		200	92.27	87.16	80

Unless indicated otherwise, the current density was 20 mA cm^{-2}, deposition time 1 h, the solution was 1.25 M $ZnSO_4$ and 1 M H_2SO_4

compared to the other two additives. With the addition of glutin, much smaller zinc cathodic and anodic peaks can be observed indicative of larger zinc deposition and dissolution polarization. With the combined additive, SLS and Sb(III), almost no change in the cyclic voltammograms for zinc electrodeposition and dissolution is found. It may be associated with the cathodic depolarization of Sb(III) [24].

Figure 6 shows the effect of initial scan potentials on cyclic voltammograms of zinc electrodeposition and dissolution in electrolyte without additives and with the three-selected additives. When the initial potential is successively shifted from −0.8 to −1.2 V (vs. $Hg|Hg_2SO_4$), zinc cathodic and anodic peaks consequently increase to different extents apart from with glutin. The reason possibly is that higher the initial potential, the less deposited zinc which is not stripped remains on the substrate electrode. When the initial potential is as low as −1.2 V versus $Hg|Hg_2SO_4$, so much deposited zinc remains on the substrate that the deposition of zinc needs less energy on the freshly zinc surface on the next scanning. As a result, zinc cathodic and anodic peaks increase. But, in the case of glutin, a significant increase of zinc cathodic and anodic peaks is not presented when the initial potential is shifted to a more negative value. It is possibly attributed to the strong blocking effect and adsorption of glutin. It is noteworthy that when the initial potential is −0.8 V versus $Hg|Hg_2SO_4$, a small anodic peak can be observed with the addition of indium oxide as shown in the inset of Fig. 6d. The peak should be attributed to the indium oxidation process. The cathodic peak of indium is not found possibly owing to the occurrence of the zinc and indium co-deposition. It can also explain why no nucleation loop appears on the cyclic voltammogram with indium oxide.

3.2 Zinc half-cell efficiencies in a three-electrode cell

Aiming to achieve the optimum electrolyte compositions and operating conditions for a zinc-based flow battery in sulfuric acid medium, the electrodeposition and stripping of zinc were carried out over a wide range of concentrations of Zn(II) and H_2SO_4, applied current densities and electrolytical additives in a three-electrode system with magnetic stirring. Unless indicated otherwise, the electrolyte composition was 1.25 M zinc sulfate in 1 M sulfuric acid. Electrodeposition of zinc on a graphite–resin composite substrate was carried out at 20 mA cm^{-2} for 1 h and room temperature of 25 °C. Table 3 summarizes the estimated half-cell efficiencies of the zinc electrode in terms of voltage, charge, and energy at different current density.

Figure 7a–d shows the effect of current density, the concentration of acid and zinc ions, electrolytical additives, respectively, on the charge–discharge curves of the zinc half-cell reaction. The corresponding data are listed in Table 3. In the absence of additives, the curves in Fig. 7a

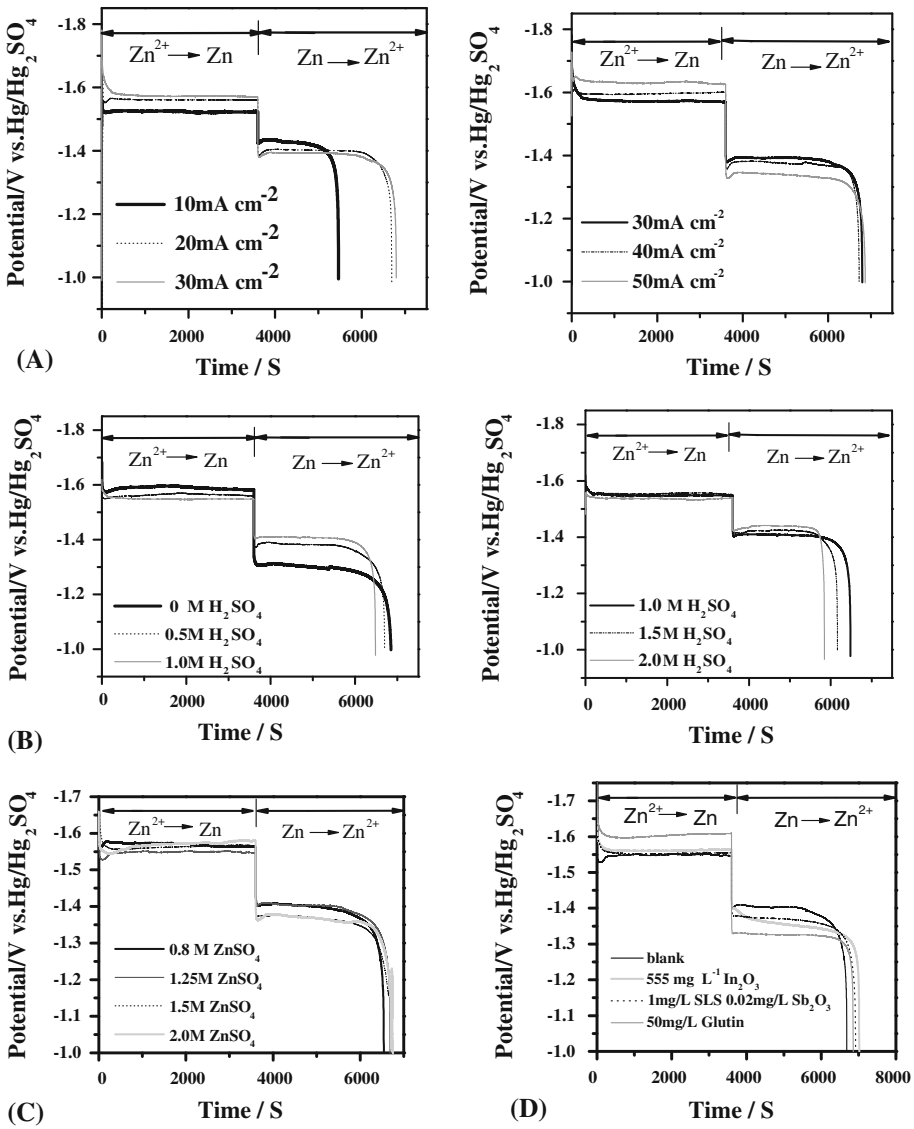

Fig. 7 The effect of current density (**a**), the concentration of acid (**b**) and zinc ions (**c**), additives (**d**) of zinc half-cell on a graphite–resin composite substrate from a sulfuric acid bath in a three-electrode cell with magnetic stirring. Unless indicated, the current density was 20 mA cm^{-2}, deposition time 1 h, room temperature of about 25 °C, and the solution was 1.25 M $ZnSO_4$ + 1 M H_2SO_4

show that larger energy efficiencies of 76–78 % are obtained at a current density range of 20–30 mA cm^{-2} (Table 3). This high efficiency was attributed to the relatively higher charge efficiency and lower potential drop. The self-discharge of zinc is rather significant during discharging at a low current density of 10 mA cm^{-2}, leading to a low charge efficiency. At higher applied current density, the charge efficiencies were found to be higher indicative of relatively small self-discharge of zinc. But the potential drop becomes larger, resulting in a decrease in energy efficiency.

Figure 7b, c shows the electrode potential versus time at different concentrations of acid and zinc ions during reduction and oxidation of zinc. The highest energy efficiency was obtained in 1–1.5 M sulfuric acid solution. Further increase of the sulfuric acid leads to a sharp drop in charge and energy efficiencies. This optimized value of H_2SO_4 concentration is consistent with that in the above cyclic voltammograms in Fig. 3. But from the cyclic voltammogram, a drastic decrease in peak current density is not observed when the H_2SO_4 concentration is increased from 1.5 to 2.0 M possibly due to instant deposition and dissolution of zinc during potential scanning. From the potentiodynamic study (log *i*–*E*) in Fig. 4, it can be seen that the exchange current density of zinc deposition and dissolution is enhanced with increasing the concentration of H_2SO_4, especially from 0 to 0.5 M. Thus, the overpotential of zinc deposition is the largest in the absence of sulfuric acid. A lower potential drop and higher voltage efficiency are obtained when the H_2SO_4 concentration is increased. However when the H_2SO_4 concentration is too high such as 2 M, a large decay in charge efficiency is observed due to the more dominant hydrogen evolution reaction and faster corrosion rate.

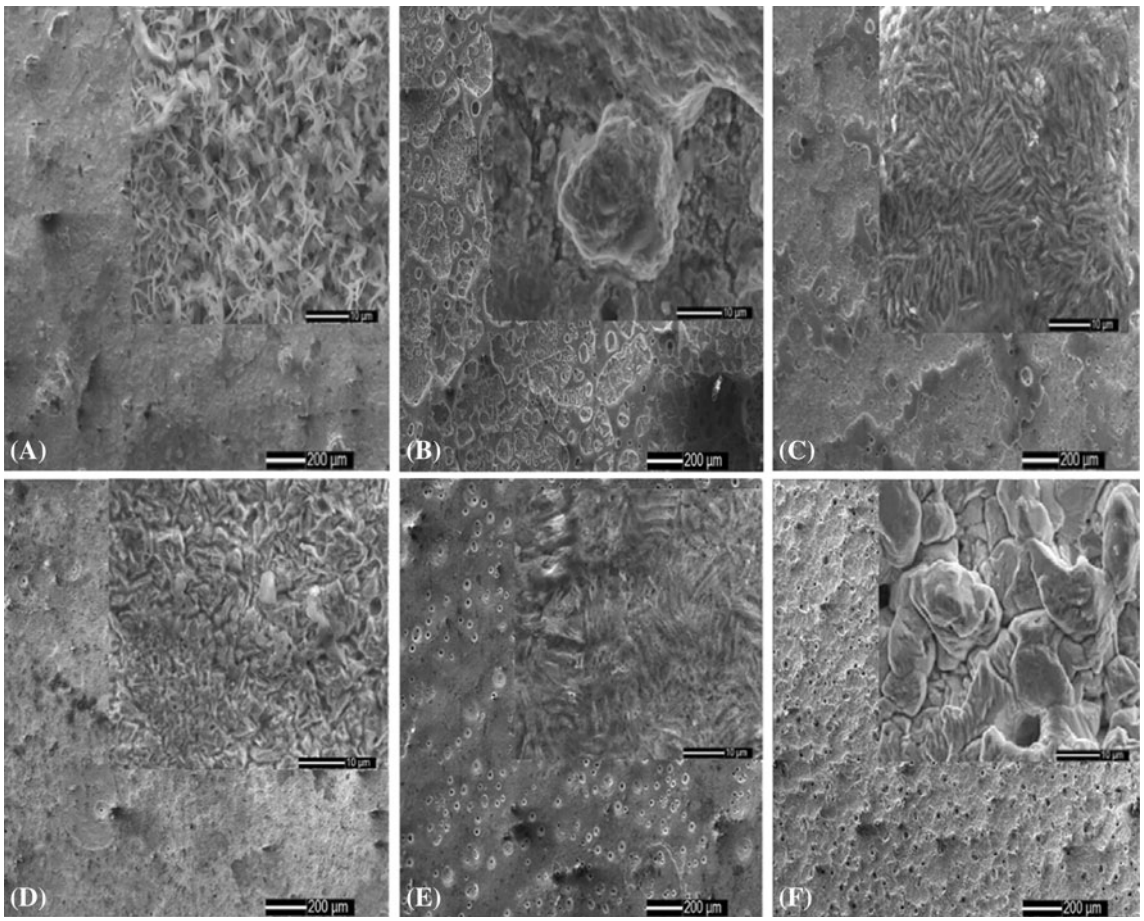

Fig. 8 SEM micrographs of the zinc electrodeposits obtained on a graphite–resin composite electrode in the absence of acid and additives (**a**), and in the presence of 1 M H_2SO_4 (**b**), 2 M H_2SO_4 (**c**), and containing 50 mg L^{-1} glutin (**d**), 1 mg L^{-1} SLS and 0.02 mg L^{-1} Sb (III) (**e**), and 555 mg L^{-1} indium oxide (**f**) in 1 M H_2SO_4 medium. Electrolyte compositions and operating conditions were as in Fig. 7

The change of zinc ion concentration influences the energy efficiency to a certain extent as shown in Fig. 7d. As an increase in zinc ion concentration facilitates the diffusion mass-transfer, the charge efficiency is improved. But when the zinc ion concentration is above 1.25 M, the energy efficiency is reversely decreased to a slight extent owing to lower electrical conductivity of electrolyte resulting from the high viscosity. Thus, zinc ion concentration of 1.25 M is preferred.

Charge–discharge experiments were also carried out in the presence of the above-selected additives at their optimized concentration values. The electrode potential during the charge/discharge cycle is shown in Fig. 7d. With the addition of additives, the charge efficiencies are improved significantly from 85.7 % without additive to over 90 % (Table 3). However, in the case of glutin, too low voltage efficiency and large potential drop are obtained. As a result, the energy efficiency is reduced compared with the additive-free electrolyte. For the other two additives, the voltage efficiencies are just slightly lowered. Thus, the energy efficiency is increased to above 80 %.

3.3 Morphologies of zinc deposits

Figure 8a–f shows the microstructures of the zinc electrodeposits from 1.25 M Zn(II) ions in H_2SO_4 solution of various concentrations and using different additives in 1 M H_2SO_4 medium. It can been seen that small pits and pin hole formation presumably as a result of the hydrogen evolution, are apparent to different degrees on the surface of zinc deposits. The higher the H_2SO_4 concentration, the more distinct this phenomenon is. In the acid-free solution, the deposit is relatively compact with few pin holes. The microstructure is formed by the needle shape grains (Fig. 8a). Similar features were observed by Gomes et al. [21] for the zinc electrowinning from acidic zinc sulfate solutions in the presence of CTAB. This indicates the competition between nucleation and crystal growth. The

morphology is associated with a strong deposition polarization. Such blocking effect may result in a large polarization and low voltage efficiency, which is demonstrated by charge–discharge experiments. In 1 and 2 M H_2SO_4 solution, the coat of zinc deposits presents more pin holes due to more serious hydrogen evolution. The morphology of zinc deposit changes to an irregular plate-like and boulder-like structure indicative of lower utilization of the current. The zinc crystals are poorly defined. It is different from the literature [15] possibly owing to the different substrates and current density used. This zinc deposit morphology causes the electrochemical activity of the zinc electrode to be enhanced as suggested in the voltammetry study. It is also confirmed by the higher voltage efficiency in the charge and discharge experiments.

With the addition of glutin in 1 M H_2SO_4 medium, the dense zinc deposits with few pin holes was observed as in the absence of acid (see Fig. 8d). The deposited zinc become fine grained with much smaller crystals. Similar morphology is also observed in the literature [13]. The strong blocking effect and adsorption of glutin are examined by the low voltage efficiency in the deposition and stripping experiment in the three-electrode system. In the presence of SLS and Sb(III), randomly oriented crystallites are distributed on the porous surface of the deposits (Fig. 8e). Tripathy et al. [24] observed the similar morphology. Presence of Sb(III) in the electrolyte causes depolarization of the cathode, whereas presence of SLS in the electrolyte polarizes the cathode. A combination of both could obtain an optimum result for the electrochemical performance of zinc deposition and dissolution in sulfate solution. Such synergistic effect maybe results in a lower overpotential and relatively high energy efficiency, which is demonstrated by charge–discharge experiments. Among the additives tested, indium oxide has the highest charge efficiency and a significant enhancement in energy efficiency. Due to the low deposition overpotential, zinc deposits at a faster rate and more irregular boulder-like agglomerates (see Fig. 7f) are observed after the addition of indium oxide. The similar microstructure was also observed in the literatures [7] and [25]. The high charge efficiency could be attributed to the high H_2 overpotential on the pre-deposited metal, indium, as shown in Fig. 6d.

4 Conclusion

Zinc electrodeposition from 0.01 M Zn(II) ions in a sulfate bath is a mass transport controlled process and a quasi-reversible reaction with a zinc ion diffusion coefficient of 4.6×10^{-6} cm^2 s^{-1} obtained.

The increase of acid concentration facilitates an improvement in the kinetics of zinc deposition–dissolution process, obtaining higher energy efficiencies. But too high acid concentration would result in a significant decrease in charge efficiency due to more dominant hydrogen evolution and faster corrosion rate. Although higher zinc ion concentration was beneficial for a redox flow battery application, the energy efficiency is reversely decreased to a slight extent at zinc ion concentration above 1.25 M. The optimum electrolyte compositions for zinc-based flow battery application were suggested at high Zn(II) concentration (1.25 M) and at moderate sulfuric acid concentration (i.e., 1.0–1.5 M) at a current density range of 20–30 mA cm^{-2}.

In the presence and absence of H_2SO_4 or electrolytical additives tested, no dendrite was observed in all zinc electrodeposits at 20 mA cm^{-2} for 1 h. The low deposition overpotential observed in 1–1.5 M H_2SO_4 medium. With the addition of 555 mg L^{-1} indium oxide or 1 mg L^{-1} SLS and 0.02 mg L^{-1} Sb(III) combined additive in 1 M H_2SO_4 solution, the zinc electrodeposition overpotential is just increased a bit with irregular plate-shaped and boulder-like microstructures on the porous surface of deposits. Among the three additives tested, both indium oxide and SLS–Sb(III) combined additive are suitable for zinc-based redox flow batteries as energy efficiency improved from 77 % in the absence of additives to over 80 % .

Acknowledgments This work was financed by the National Basic Research Program (973 Program) of China (2010CB227204).

References

1. Huang KL, Li XG, Liu SQ (2008) Renew Energy 33:186
2. Yu JX, Yang HX, Ai XP (2001) J Power Sources 103:93
3. Butler PC, Eidler PA, Grimes PC, Klassen SE, Miles RC (1994) In: Linden D (ed) Handbook of batteries, 3rd edn. McGraw Hill, New York
4. Cheng J, Zhang L, Yang YS, Wen YH (2007) Electrochem Commun 9:2639
5. Wen YH, Cheng J, Ning SQ (2009) J Power Sources 188:301
6. Zhang L, Cheng J, Yang YS (2008) J Power Sources 179:381
7. Leung PK, Ponce de León C, Low CTJ, Walsh FC (2011) Electrochim Acta 56:6536
8. Leung PK, Ponce de León C, Low CTJ, Walsh FC (2011) Electrochim Acta 56:2145
9. Leung PK, Ponce de León C, Low CTJ, Shah AA, Walsh FC (2011) J Power Sources 196:5174
10. DiAZ-Arista P, Meas Y, Ortega R, Trejo G (2005) J Appl Electrochem 35:217
11. Trejo G, Ortega RB, Meas YV, Ozil P, Chainet E, Nguyen B (1998) J Electrochem Soc 145:4090
12. Yu JX, Chen YY, Yang HX, Huang QA (1999) J Electrochem Soc 146:1789
13. Saba AE, Elsherief AE (2000) Hydrometallurgy 54:91
14. Gomes A, da Silva Pereira MI (2006) Electrochim Acta 52:863
15. Alfantazi AM, Dreisinger DB (2003) Hydrometallurgy 69:99
16. Gomes A, Viana AS, da Silva Pereira MI (2007) J Electrochem Soc 154:D452
17. Gomes A, da Silva Pereira MI (2006) Electrochim Acta 51:1342
18. Youssef KMS, Koch CC, Fedkiw PS (2004) J Electrochem Soc 151:C103

19. Fang B, Iwasa S, Wei Y, Arai T, Kumagai M (2002) Electrochim Acta 47:3971
20. Fletcher S, Halliday CS (1983) J Electroanal Chem 159:267
21. Yu JX, Yang HX, Ai XP, Chen YY (2002) Russ J Electrochem 38:321
22. Zhang QB, Hua YX (2009) Hydrometallurgy 99:249
23. Saba AE, Elsherief AE (2000) Hydrometallurgy 54:91
24. Tripathy BC, Das SC, Misra VN (2003) Hydrometallurgy 69:81
25. Gomes A, da Silva Pereira MI (2006) Electrochim Acta 51:1342